

Raman scattering study of the long-wavelength longitudinal-optical-phonon–plasmon coupled modes in high-mobility InN layers

Ramon Cuscó, Jordi Ibáñez, Esther Alarcón-Lladó, and Luis Artús

Institut Jaume Almera, Consell Superior d'Investigacions Científiques (CSIC), Lluís Solé i Sabarís s.n., 08028 Barcelona, Spain

Tomohiro Yamaguchi and Yasushi Nanishi

Faculty of Science and Engineering, Ritsumeikan University, 1-1-1 Noji-Higashi, Kusatsu, Shiga 525-8577, Japan

(Received 20 January 2009; revised manuscript received 17 March 2009; published 24 April 2009)

We have studied the longitudinal-optical (LO)-phonon–plasmon coupled modes in high-mobility InN layers with free-electron densities ranging from 2.3×10^{18} to 1.6×10^{19} cm^{-3} by means of Raman scattering. The observed L^- coupled-mode peak displays the usual behavior for the low energy branch of the long-wavelength coupled modes, increasing in frequency and phononlike character as the electron density increases. The L^- mode behavior can be satisfactorily explained by the standard dielectric model developed by Hon and Faust which takes into account wave-vector conserving scattering processes governed by the dipole-allowed deformation potential and electro-optic mechanisms. The free-electron density obtained from line-shape fits to the L^- peak agrees well with Hall-effect measurements. The E_2^{high} mode shifts to lower frequencies as the electron density increases, suggesting that strain relaxation has a bearing on the residual electron density in the InN layers. The L^- frequency exhibits also a dependence on the excitation wave vector, which further indicates that wave-vector conserving scattering by LO-phonon–plasmon coupled modes takes place in these high-mobility samples. The presence of a relatively strong LO signal is attributed to surface-field-induced scattering in the accumulation region.

DOI: [10.1103/PhysRevB.79.155210](https://doi.org/10.1103/PhysRevB.79.155210)

PACS number(s): 78.30.Fs, 63.20.kk

I. INTRODUCTION

Owing to its narrow band gap and superior transport properties (small effective mass, high electron mobility, and high drift velocity), InN is currently attracting much attention as a promising candidate to develop novel optical and high-frequency device applications. InN is also remarkable among III-V semiconductors because it exhibits surface electron accumulation,^{1–3} which, besides affecting the optical and transport properties of InN, could be exploited to realize hybrid superconductor/semiconductor devices.⁴

Over the last few years, efforts have been concentrated in producing high-quality InN films. The availability of InN epilayers with improved crystalline quality is decisive in order to achieve high performance devices and also to investigate the fundamental properties of this compound. Raman spectroscopy is a well-suited technique to characterize the crystal quality and the strain state of semiconductor compounds and structures. The study of longitudinal-optical (LO)-phonon–plasmon coupled modes (LOPCMs) by Raman scattering allows the free-carrier density to be determined in a contactless way in polar semiconductors.^{5–7} When suitable models are utilized to analyze the Raman spectra, a good agreement is generally found between Raman scattering determinations of the free-charge density and the results of Hall effect⁶ and magnetotransport measurements.⁸

Despite much work dealing with Raman scattering in n -type InN layers,^{9–17} there is an ongoing controversy over the nature of the LOPCMs in this compound. Several authors reported the observation in bulk, heavily doped n -type InN epilayers of a single $A_1(\text{LO})$ -like structure that was ascribed to LOPCMs and invoked wave-vector nonconserving scattering processes to explain their results.^{13,14,16,17} Following this

analysis, some of the authors concluded that the dominant scattering mechanism in their samples was the forbidden impurity-induced Fröhlich mechanism^{13,16} whereas others discarded the impurity-induced Fröhlich mechanism in favor of the charge-density fluctuation mechanism.¹⁴ On the other hand, several authors observed Raman features close to the $A_1(\text{TO})$ mode of bulk InN that they assigned either to $A_1(\text{TO})$ modes^{10,13,17} or to L^- coupled modes.^{9,11,12,15} Recently, the observation of L^- coupled modes has been reported in InN nanocolumns.¹⁸ In general, little evidence is provided to conclusively demonstrate the presence of L^- peaks in the Raman spectra of n -type InN, and a number of authors attribute the features reported below the $A_1(\text{TO})$ phonon mode to disorder-activated modes (see, for instance, the discussion in Ref. 14). Most of the assignments of Raman peaks to the L^- LOPCMs in InN have been performed based on the isolated observation of an additional peak in a given sample. A systematic study and analysis of the L^- mode behavior in InN samples with different carrier concentrations is still lacking. More work is thus required to clarify the issue of LO-phonon–plasmon coupling in the Raman spectrum of n -type InN.

In the present work we use Raman scattering to study a series of unintentionally doped, n -type InN epilayers with free-electron densities spanning a 1 order of magnitude range, from $N_e \approx 2 \times 10^{18}$ to $N_e \approx 2 \times 10^{19}$ cm^{-3} . The Raman spectra of all the samples are dominated by the E_2^{high} and $A_1(\text{LO})$ modes of InN. We discuss the frequency dependence of the E_2^{high} mode in our InN epilayers as a function of N_e . Our experiments reveal the presence of a Raman peak at frequencies below that of the forbidden $A_1(\text{TO})$ mode that exhibits a clear upward frequency shift with increasing N_e . This peak can be unambiguously assigned to an L^- LOPCM

TABLE I. Details of the *n*-InN epilayers studied in this work: film thickness d , full width at half maximum (FWHM) of the (002) x-ray diffraction peak, electron density N_e^{Hall} and mobility μ_{Hall} as determined from Hall measurements, and electron density N_e^{Raman} and phenomenologic electronic damping Γ_e as obtained from the analysis of the Raman spectra. All of the InN films were grown on sapphire substrates, except for sample A1 which was grown on a GaN template on sapphire. Samples B1 and B2 were grown in a different MBE system.

Sample	d (nm)	FWHM (arcmin)	N_e^{Hall} (10^{18} cm $^{-3}$)	μ_{Hall} (cm 2 V $^{-1}$ s $^{-1}$)	N_e^{Raman} (10^{18} cm $^{-3}$)	Γ_e (cm $^{-1}$)
A1	550	9.6	2.3	1440		
A2	1000	2.4	4.3	1090	4.2	116
A3	750	2.5	5.8	930	5.2	113
A4	250	2.1	6.9	900	5.6	97
B1	400	0.8	6.5	954	6.6	76
B2	400	1.0	16	684	20	57

arising from coupling to the bulk-electron plasmons. Raman measurements excited with visible and near-infrared (NIR) radiation allow us to demonstrate the wave-vector dispersion of the observed L^- mode. We find that, as expected for the L^- branch of LOPCMs, the L^- peak shifts to higher frequencies when the excitation wavelength is reduced from 780.0 to 514.5 nm. We perform a line-shape analysis of the Raman spectra based on the Lindhard-Mermin model to evaluate the bulk-electron concentration in our samples. The values thus obtained agree well with Hall-effect measurements, which ultimately corroborates that the L^- peaks arise from coupling to the bulk-electron plasmons. The origin of the observed LO modes is also discussed.

II. EXPERIMENT

Six nominally undoped InN epilayers were grown at ~ 500 °C by plasma-assisted molecular-beam epitaxy (MBE). The samples were grown in two different MBE systems and are labeled accordingly as A (samples A1–A4) and B (samples B1 and B2). All of the samples were deposited on nitridated (0001) sapphire substrates except sample A1, which was grown on a GaN/sapphire template. The thickness d of the InN films is in the 250–1000 nm range (see Table I). Electrical characterization of the samples was performed by standard Hall measurements, which showed that all of the samples display *n*-type conductivity with free-electron densities ranging from 2.3×10^{18} to 1.6×10^{19} cm $^{-3}$ and Hall mobilities μ_{Hall} from 684 to 1440 cm 2 V $^{-1}$ s $^{-1}$. Free-electron densities and Hall mobilities are summarized in Table I. Raman scattering experiments were carried out at 80 K in a $z(x, \cdot)\bar{z}$ backscattering configuration, where z is parallel to the c axis. For these measurements, excitation wavelengths $\lambda_{\text{exc}} = 514.5$ nm (Ar $^+$ laser) and 780.0 nm (Ti-sapphire laser) were used. The Raman spectra were recorded using a Jobin Yvon T64000 spectrometer equipped with a charge coupled device (CCD) detector cooled with liquid nitrogen. For the visible measurements, the subtractive configuration of the spectrometer was employed, with 100 μm slits. For the NIR experiments, we used the single stage of the spectrometer together with a razor-edge filter and 200 μm slits.

According to the absorption coefficient of InN measured by Kasic *et al.*¹⁹ in the 0.5–2.0 eV spectral region, the Raman probing depth for the 780.0 nm excitation is $1/2\alpha = 72$ nm. By extrapolation of the data of Ref. 19 to 2.41 eV, we estimate a Raman probing depth of ≈ 36 nm for the 514.5 nm excitation. Therefore, although InN is strongly absorbing to incident radiation in both cases, in our Raman measurements the penetration depth of the NIR excitation is nearly twice as large as that of the visible excitation.

III. THEORY

A. General considerations

In doped polar semiconductors, free-charge excitations couple with polar optical modes via their respective macroscopic electric fields giving rise to LOPCMs. In heavily doped samples with high mobility, the L^+ branch of the LOPCMs usually exhibits a plasmonlike character whereas the L^- branch is phononlike and its frequency approaches that of the TO mode.⁵ Several mechanisms may contribute to light scattering by LOPCMs. On the one hand, the deformation potential (i.e., modulation of the crystal potential by the atomic displacements) and the electro-optic interaction (i.e., the interband matrix elements of the Fröhlich interaction involving the macroscopic electric fields associated with the LOPCMs) provide the dipole-allowed scattering mechanisms for scattering by LOPCMs which are dominant away from electronic resonances. On the other hand, the intraband matrix elements of the Fröhlich interaction yield a q -dependent contribution to the Raman polarizability which is strongly enhanced near electronic resonances. In the usual backscattering geometry on a (0001) face of the wurtzite structure, the $E_1(\text{LO})$ mode is symmetry forbidden whereas the $A_1(\text{LO})$ mode is allowed in the $z(xx)\bar{z}$ configuration. Then, both the dipole-allowed and the Fröhlich mechanisms contribute with the same symmetry to the Raman scattering by longitudinal modes polarized along z , and therefore, unlike the case of the zinc-blende structure, these two mechanisms cannot be separated by selecting a suitable polarization configuration. A further channel for “forbidden” LO scattering is the surface-field-induced scattering, which is related to the

separation of electron and holes in the intermediate states induced by the built-in electric field of the space-charge region.²⁰ It should be stressed that this effect can be important in InN since this semiconductor exhibits the largest native electron accumulation observed at a III-V surface, giving rise to surface electric fields of $\sim 4.6 \times 10^3$ kV cm⁻¹.² Additionally, another scattering process by plasmons which is associated with the charge-density fluctuations of the electron gas exists near the E_0 and $E_0 + \Delta_0$ gaps.⁵

Kuball *et al.*²¹ observed an enhancement of the $A_1(\text{LO})$ intensity as the excitation wavelength was increased up to 830 nm and suggested the existence of a critical point at around 1.2–1.3 eV. The 514.5 nm excitation used in our Raman experiments is well away from that possible critical point so that we may consider the measurements to be off resonance, although the relatively strong LO signal indicates some residual resonant enhancement. On the other hand, we observe a noticeable increase in the LO signal relative to the E_2^{high} mode for the 780 nm excitation, which indicates a significant contribution of the Fröhlich mechanism in this case. In contrast, the charge-density fluctuation mechanism appears to be negligible for the analysis of our spectra. A rough estimation of the line shape to be expected from charge-density fluctuations using the expressions of Ref. 22 indicates that the intensity of the plasmonlike L^+ mode should be significantly higher than that of the phononlike L^- mode, contrary to our experimental results where only the L^- mode can be unambiguously detected.

B. Line-shape model

In this work we are mainly concerned with the modeling of the charge-density dependence of the L^- mode observed in our samples. For simplicity, we neglect absorption effects and consider only the deformation potential and electro-optic scattering mechanisms. As discussed in Sec. II, this is a reasonably good assumption for the 514.5 nm excitation. However, for the 780 nm excitation, the Fröhlich mechanism yields a significant contribution to the Raman signal and, since the Raman polarizabilities are complex in the intrinsic absorption region, interference between the different scattering mechanisms may take place.^{23,24} Although we expect these effects to have only a minor influence on the L^- line shape, we rely on the Raman spectra excited with the 514.5 nm line to determine the electron density from the L^- line-shape fit. To model the L^- peak we apply the standard dielectric theory in the formalism of Hon and Faust.²⁵ This model has been highly successful in describing LOPCMs in other narrow band gap III-V semiconductors.^{6,26}

In the fluctuation-dissipation formalism developed by Hon and Faust,²⁵ the differential Raman cross section for the dipole-allowed scattering by LOPCMs can be expressed as

$$\frac{\partial^2 \sigma}{\partial \omega \partial \Omega} \propto [n(\omega) + 1] \Im \left\{ \frac{-1}{\varepsilon(q, \omega)} \left[\frac{\varepsilon_\infty}{4\pi} + 2A\chi_I - A^2\chi_I \left(1 + \frac{4\pi}{\varepsilon_\infty} \chi_e \right) \right] \right\}, \quad (1)$$

where $\varepsilon(q, \omega) = \varepsilon_\infty + 4\pi(\chi_I + \chi_e)$ is the total dielectric function of the coupled plasma–ionic-lattice system,

$$\chi_I = \frac{\varepsilon_\infty}{4\pi} \frac{\omega_{\text{LO}}^2 - \omega_{\text{TO}}^2}{\omega_{\text{TO}}^2 - \omega^2 - i\Gamma_I \omega} \quad (2)$$

is the ionic-lattice susceptibility, and χ_e is the wave-vector- and frequency-dependent electronic susceptibility.^{5,6} In Eq. (1), $n(\omega)$ is the Bose-Einstein distribution function and $A = \omega_{\text{TO}}^2 C / (\omega_{\text{LO}}^2 - \omega_{\text{TO}}^2)$, where C is the Faust-Henry coefficient and ω_{TO} and ω_{LO} are the zone-center transverse and longitudinal-optical-mode frequencies, respectively. We assume wave-vector conservation in the backscattering process so that $q = 4\pi n / \lambda_{\text{exc}}$, where n is the refractive index.

We evaluate the free-carrier susceptibility χ_e using the Lindhard-Mermin model

$$\chi_e(q, \omega) = \frac{(1 + i\Gamma_e/\omega)\chi_e^L(q, \omega + i\Gamma_e)}{1 + i\Gamma_e\chi_e^L(q, \omega + i\Gamma_e)/[\omega\chi_e^L(q, 0)]}, \quad (3)$$

where Γ_e is a phenomenological collision damping constant and the Linhard susceptibility $\chi_e^L(q, \omega)$ is given by

$$\chi_e^L(q, \omega) = \frac{e^2}{2\pi^3 q^2} \int f(E_F, T, k) \frac{E(\mathbf{q} + \mathbf{k}) - E(\mathbf{k})}{[E(\mathbf{q} + \mathbf{k}) - E(\mathbf{k})]^2 - (\hbar\omega)^2} d^3k. \quad (4)$$

In Eq. (4), $f(E_F, T, k)$ is the Fermi-Dirac distribution function and $E(\mathbf{k})$ is the conduction band dispersion. Owing to its narrow band gap, the conduction band of InN shows a strong nonparabolicity.²⁸ This is taken into account through a simplified two-band Kane's model.³⁰ In the small effective-mass limit and neglecting spin-orbit interaction the conduction band dispersion is given by

$$E(k) = \frac{E_G}{2} \left[\sqrt{1 + \frac{4\hbar^2 k^2}{E_G 2m^*}} - 1 \right], \quad (5)$$

where E_G is the band-gap energy and m^* is the band-edge electron effective mass. The values of the model parameters used in the calculations are listed in Table II.

IV. RESULTS AND DISCUSSION

A. The Raman spectra of n -InN epilayers

A typical spectrum of the InN epilayers (sample A2) is displayed in Fig. 1. A weak background signal which may be related to surface roughness and some residual luminescence is present in all of the samples. The spectrum is dominated by the E_2^{high} peak at ≈ 495 cm⁻¹, and a relatively strong $A_1(\text{LO})$ peak is also observed at ≈ 593 cm⁻¹. A weak peak is detected at ≈ 402 cm⁻¹ which, as our analysis below will demonstrate, can be unambiguously assigned to the L^- branch of the LOPCMs. The Raman spectra of these samples display two unexpected characteristics for LOPCM spectra, namely, the absence of the L^+ mode and the presence of a strong unscreened $A_1(\text{LO})$ mode. The absence of the L^+ peak can be explained by the inhomogeneous broadening induced by fluctuations of the electron density across the crystal. These affect predominantly the L^+ since for the electron densities of our samples the L^+ has a plasmonlike character and therefore its frequency is more sensitive to charge-density variations as compared to the phononlike L^- mode. This

TABLE II. Input parameters for the LOPCM line-shape model.

Symbol	Description	Value	Ref.
ω_{LO}	$A_1(LO)$ frequency	591.8 cm^{-1}	9 and 27 ^a
ω_{TO}	$A_1(TO)$ frequency	451.3 cm^{-1}	9 and 27 ^a
Γ_I	Ionic damping constant	5 cm^{-1}	Estimated from our Raman spectra (see Sec. IV C).
m^*	Electron effective mass	0.07 m_e	28
C	Faust-Henry coefficient	-2.0	14
E_G	Band-gap energy	650 meV	19
ϵ_∞	High-frequency dielectric constant	6.7	19
n	Refractive index	2.5	29

^a80 K strain-free values estimated from data in Refs. 9 and 27 and the temperature shift observed in our samples. For the line-shape fits, these values were corrected for strain according to the E_2^{high} frequency measured in each layer using data Ref. 27 (for details, see Sec. IV B 1).

effect, which was also observed in samples with an inhomogeneous doping profile produced by ion implantation,³¹ is illustrated in Fig. 1, where we have plotted with a dotted line the LOPCM line shape calculated for $N_e=4.3 \times 10^{18} \text{ cm}^{-3}$ using the theoretical model described in Sec. III B and with a dashed line the LOPCM line shape averaged over a Gaussian distribution ($\sigma=1.5 \times 10^{18} \text{ cm}^{-3}$) of electron densities centered at N_e . Whereas for such an electron density one would expect a well-defined L^+ peak at $\approx 885 \text{ cm}^{-1}$ (dotted line), the L^+ turns out to be a weak broad band when inhomogeneous broadening is taken into account (dashed line). In contrast, the L^- peak is much less affected and it still retains its characteristic features. Considering the typical LOPCM and background signal levels of the spectra, it is not surprising that the unambiguous detection of the L^+ mode was not possible. It should be mentioned that we have not included the inhomogeneous broadening in the fits to the Raman spectra to avoid its time-consuming computational complexity.

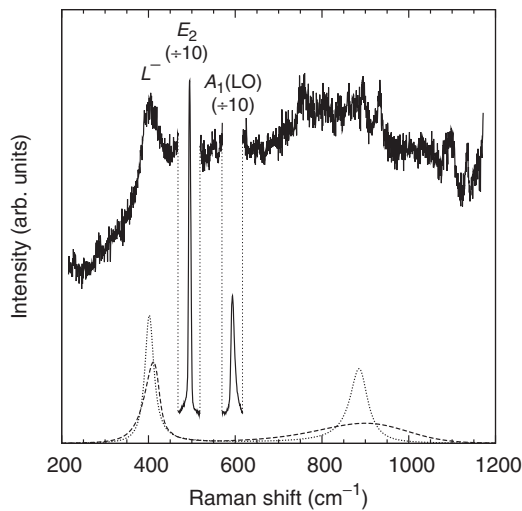


FIG. 1. Raman spectrum of sample A2 taken under 514.5-nm-wavelength excitation at 80 K. Dotted line: theoretical LOPCM line shape calculated for $N_e=4.3 \times 10^{18} \text{ cm}^{-3}$; dashed line: averaged line shape for a Gaussian distribution ($\sigma=1.5 \times 10^{18} \text{ cm}^{-3}$) of the electron density centered at N_e .

Since, as can be seen in Fig. 1, the average over a Gaussian distribution of N_e gives rise to a slight upward frequency shift of the L^- peak, neglecting the inhomogeneous broadening implies an overestimation of the electron density from the fits. However, the effect is small and fortuitously compensates in part the expected discrepancy between Raman and Hall determinations of N_e which, as we discuss below, arises from the presence of interface charge beyond the finite probing depth of the Raman experiments. The reason for the observation of a strong unscreened LO signal in degenerate samples will be discussed in Sec. IV C.

For the comparison between the Hall-derived electron densities and the Raman scattering results, two issues are to be considered. First, whereas Raman scattering by the LOPCMs probes the three-dimensional (3D) electron density in the InN films, the standard Hall-effect determination of the free-charge density contains a contribution from the two-dimensional sheet carrier density n_s in the native surface accumulation layer.³² However, the mobility of the surface accumulation electrons μ_s is typically 1 order of magnitude lower than that of the bulk electrons μ^{3D} .¹⁶ Their contribution to the measured Hall sheet density is therefore greatly reduced, and we neglect it in our analysis. Second, a significant role in producing n -type conductivity has been attributed to positively charged nitrogen vacancies formed in threading dislocations.³² This gives rise to a substantial carrier density at the InN/substrate interface. While Hall-effect determinations yield an average sheet carrier density for the whole layer, Raman scattering experiments primordially probe a region within the optical skin depth. Since dislocation density decreases away from the InN/substrate interface, the electron density probed by the Raman experiments is expected to be somewhat lower than the values derived from Hall measurements.

The role of threading dislocations in producing n -type InN layers becomes apparent in the Raman spectra of our samples. In Fig. 2 we plot the E_2^{high} frequency vs electron density for our set of samples. Representative E_2^{high} spectra are shown in the inset. A trend of decreasing E_2^{high} frequency with increasing electron concentration is clearly seen, which indicates the progressive relaxation of in-plane biaxial strain due to threading dislocations²⁷ and corroborates the contri-

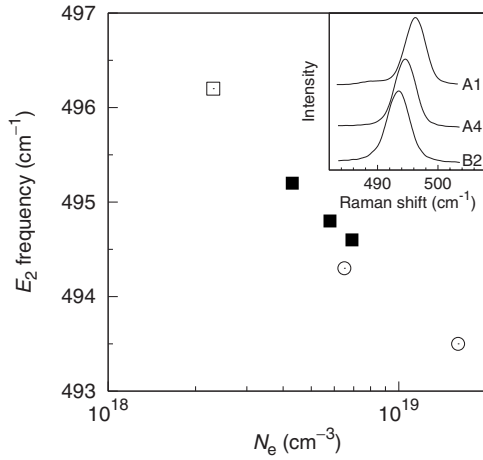


FIG. 2. E_2^{high} frequency at 80 K vs electron density for our three groups of InN epilayers. Empty square: sample A1; filled squares: samples A2–A4; circles: samples B2 and B1. Inset: representative Raman spectra of the E_2^{high} mode.

bution of positively charged dislocations to the free-electron density in InN epilayers.³²

B. The L^- coupled modes

1. Free-electron density determination

Figure 3 shows the L^- spectral region of the Raman spectra obtained at 80 K from the InN samples with different free-electron densities studied in this work. The spectrum of sample A1 is not included because no unambiguous L^- signal could be detected in that particular sample. As can be seen in Fig. 3, in the free-electron density range studied the frequency of the L^- Raman peak exhibits a substantial upward shift (~ 40 cm^{-1}) as N_e increases. The high sensitivity of the

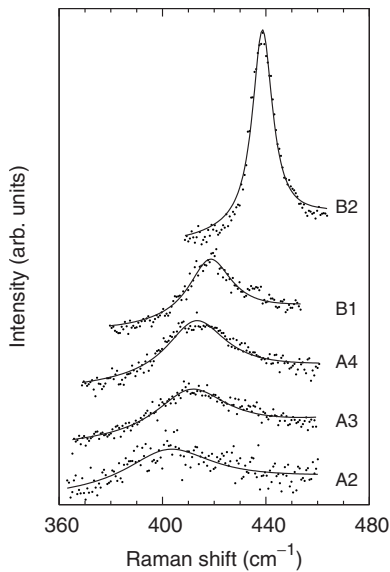


FIG. 3. Raman spectra (dots) of the L^- coupled modes of the n -type InN epilayers taken under 514.5-nm-wavelength excitation at 80 K. Solid lines are fits of the line-shape model described in Sec. IV B to the Raman spectra.

L^- mode to changes in N_e makes it suitable to be used as a probe of the free-electron density in InN. Here we employ the theoretical model described in Sec. IV B to fit the L^- Raman spectra excited with the 514.5 nm line and thus obtain the electron-density determination from the Raman measurements. The parameters used in the model are listed in Table II. Since in the samples with higher electron densities the L^- mode displays a substantial phononlike character and its frequency approaches that of the $A_1(\text{TO})$ mode, it is important to use accurate values of the $A_1(\text{TO})$ frequency in the line-shape fit calculations. As discussed in Sec. III, the E_2^{high} frequency shifts observed in our Raman spectra reveal that different levels of residual biaxial strain exist in the set of InN epilayers studied, and therefore a correction for strain has to be introduced in their respective $A_1(\text{TO})$ frequencies. This is carried out in the following manner. In Ref. 27, strain-free values of the E_2^{high} and $A_1(\text{LO})$ frequencies were determined at room temperature. Taking into account the deformation potentials determined for the $A_1(\text{LO})$ and E_2^{high} modes in Ref. 27, and assuming a similar strain dependence for the $A_1(\text{TO})$ mode, the strain-free $A_1(\text{TO})$ frequency is estimated to be ≈ 449 cm^{-1} from the $x(\text{zz})\bar{x}$ spectra reported in Ref. 9. Then, from the shift of the phononlike L^- peak observed in sample B2 when cooling from room temperature to 80 K, we estimate a strain-free $A_1(\text{TO})$ frequency of ≈ 451.3 cm^{-1} at 80 K. For the $A_1(\text{LO})$ frequency we take the strain-free value reported in Ref. 27 and correct it for the temperature shift that we observe in our Raman spectra. This yields a strain-free value of ≈ 591.8 cm^{-1} for the $A_1(\text{LO})$ mode at 80 K. Finally, using the dependence on biaxial strain of the $A_1(\text{LO})$ mode frequency,²⁷ the $A_1(\text{LO})$ and $A_1(\text{TO})$ frequencies were corrected for strain according to the strain state of each layer as deduced from the measured E_2^{high} frequency shifts. The resulting phonon frequency values specific to each layer were used to perform the line-shape fits.

Figure 3 shows the L^- line-shape fits of the LOPCM model (solid line) to the Raman spectra of the InN epilayers (dots). The corresponding free-electron density and electronic damping values are listed in columns 6 and 7 of Table I. The optical determination of the free-electron density in the sample with the lowest electron density (sample A1) was not possible because no reliable L^- signal could be detected. As can be seen in Fig. 3, the intensity of the L^- mode decreases as it gains in plasmonlike character with decreasing electron density. According to Hall measurements (see Table I), sample A1 has a free-electron density which is about half of that measured in sample A2. Then, taking into account the intensity trend observed in Fig. 3 and the low Raman signal level of the L^- mode, it is not surprising that no L^- Raman peak could be detected in sample A1.

For all the studied InN layers, the calculated line shapes closely match the experimental Raman spectra. As expected from long-wavelength LOPCMs, the L^- peak shifts to higher frequencies and becomes narrower and more intense with increasing free-electron density as the L^- branch gains in phononlike character. The good accord between the line-shape model and the experiment is evidence that wave-vector conserving Raman scattering by long-wavelength LOPCMs does take place in the InN layers investigated. This is in contrast with several studies of LO-phonon-

plasmon coupling in n -InN layers, where wave-vector non-conservation and the participation of large wave-vector modes in the scattering process had to be invoked to account for features in the Raman spectra that were assigned to LOPCMs.^{13,14,16,17} Our results also indicate that the observed LOPCMs can be satisfactorily modeled by using the dipole-allowed deformation potential and electro-optic mechanisms, contrary to previous studies where charge-density fluctuation¹⁴ and impurity-induced Fröhlich^{13,16} mechanisms were proposed as the dominant scattering mechanisms in n -type layers.

As can be seen in Table I, the electron-density values obtained from the fits to the L^- mode agree well with those derived from Hall measurements, considering the large uncertainty values in the electron-density determination. As discussed in Sec. IV A, Raman scattering measurements are expected to yield free-electron density values lower than those determined by Hall-effect measurements. This is indeed the case for samples A2–A4. The largest deviation in this group occurs for sample A4. In this particular sample, the InN film thickness is only $d \sim 250$ nm, and therefore the relative contribution to the Hall-measured total sheet density from the positively charged nitrogen vacancies along dislocations in the region near to the interface³² is more important. In contrast, for the group B samples, the free-electron density determined by Raman measurements is higher than the one derived from Hall measurements, and the difference is significantly larger for the layer with the highest electron density (sample B2). We attribute this discrepancy to the failure of the simplified two-band Kane's model³⁰ to accurately describe the conduction band nonparabolicity at large electron wave vectors, which is probably due to the fact that the spin-orbit interaction and interactions with higher conduction bands were ignored in the model. Our results suggest that, for very high electron densities, band nonparabolicity is less pronounced than predicted by the simple $\mathbf{k} \cdot \mathbf{p}$ theory used in the line-shape model.

In contrast to the Hall mobility, which decreases as the electron density increases, the phenomenological electronic damping parameter Γ_e shows a reversed trend, i.e., Γ_e^{-1} increases with increasing electron density. This is a consequence of the inhomogeneous broadening of the L^- peaks associated with fluctuations of the free-electron density in the InN layers. The inhomogeneous broadening effect is more important in the samples with lower free-electron density (group A), where the L^- modes acquire a substantial plasmonlike character and their frequency is more sensitive to changes in the electron density. Then, although electron mobility is higher in those samples, the width of the L^- peak is enlarged by inhomogeneous broadening and does not reflect the true collision damping of the electron gas. A more representative value of Γ_e is obtained from the sample with the highest electron density (sample B2), where the L^- mode has a strong phononlike character and its width is nearly unaffected by inhomogeneous broadening. The low values of electronic damping parameter found (see Table I) suggest that in high-quality InN layers impurity-induced wave-vector nonconserving scattering are relatively unimportant for LOPCM scattering.

In Fig. 4 we compare the L^- frequencies as determined from the Raman spectra of the n -InN epilayers with the the-

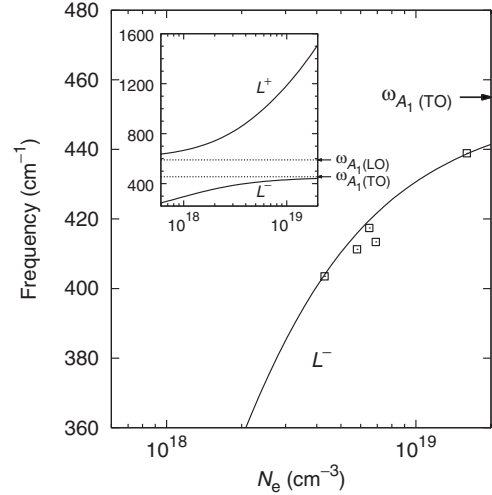


FIG. 4. Free-electron-density dependence of the L^- coupled-mode frequency as calculated from the model described in Sec. IV B. The squares represent the L^- frequencies observed in the InN epilayers plotted vs the Hall-derived electron densities. The inset displays the LOPCM frequency dispersion with electron density for both L^+ and L^- branches.

oretical frequencies calculated using the model described in Sec. IV B. In the inset we plot the dispersion of both L^+ and L^- branches with free-electron density. The curves were generated for generic values of electronic and ionic damping constants, $\Gamma_e = 50$ cm⁻¹ and $\Gamma_i = 5$ cm⁻¹, respectively, which are representative of the samples studied. Because of the low electron effective mass and the high A_1 mode frequencies of InN, for the electron-density range studied the L^- mode is still in the strong plasmon-phonon mixing regime. Over this range, the theoretical model predicts a significant shift (~ 40 cm⁻¹) for the L^- mode, which is in good agreement with the observed L^- Raman peak and the electron-density values derived from Hall measurements.

2. Wave-vector dependence

The line-shape models based on wave-vector nonconserving scattering that were applied in previous studies of LOPCMs in InN (Refs. 13, 14, 16, and 17) entail a weighted average over wave vectors ranging from zero to several times the Thomas-Fermi wave vector. The resulting line shape is thus independent of the excitation wave vector. In the present work, we have investigated the wave-vector dependence of the L^- modes in our InN layers by using 780-nm-wavelength excitation. The corresponding Raman spectra at 80 K are shown with dots in Fig. 5, where the solid lines are line-shape fits that are intended to serve as guides to the eyes. This excitation energy lies closer to a critical point (see discussion in Sec. III A), which gives rise to a resonant enhancement of the polar modes. This can be seen in Fig. 5, where we have also plotted with dotted lines the L^- line shapes corresponding to the fits to the spectra excited with the 514.5 nm line. To demonstrate the resonant enhancement of the polar modes, the intensities of all the Raman spectra were scaled to give the same E_2^{high} intensity. As can be seen in Fig. 5, the relative intensity of the L^- modes is about three

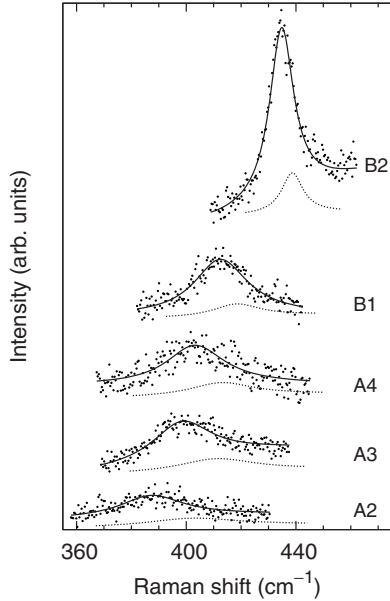


FIG. 5. Raman spectra (dots) of the L^- modes in InN epilayers taken under 780-nm-wavelength excitation at 80 K. Solid lines are line-shape fits intended to serve as a guide to the eyes. The dotted lines are the corresponding L^- line shapes fitted to the 514.5 nm spectra. To demonstrate the resonant enhancement of the L^- mode under 780 nm excitation, the intensities of all the spectra were scaled to yield the same intensity for the nonpolar E_2^{high} mode (not shown).

times higher for the NIR excitation. The frequency of the L^- modes is visibly lower in the spectra recorded under 780 nm excitation than in those excited with the 514.5 nm excitation, and the difference increases as the free-charge density decreases. This is the expected behavior for the LOPCMs when the wave-vector dispersion of the plasma oscillations is taken into account. Although the model described in Sec. IV B does predict a downward frequency shift of the L^- modes as $q=4\pi n/\lambda_{\text{exc}}$ is reduced by changing $\lambda_{\text{exc}}=514.5$ nm to $\lambda_{\text{exc}}=780.0$ nm, the observed shift is somewhat larger. It should be noted that the scattering cross section given by Eq. (1) is strictly valid only under off-resonance conditions, and this is not the case for the spectra taken under 780.0 nm excitation, as indicated by the noticeable resonant enhancement of the longitudinal polar modes. The line-shape fits displayed in Fig. 5 (solid lines) were performed with the off-resonance model (Sec. III B) and are therefore intended to serve only as guides to the eyes. In fact, the free-electron densities required to produce these fits are consistently lower than those obtained from the visible excitation fits. As already discussed above, interference between scattering mechanisms can take place near an electronic resonance, and this may slightly modify the line shape. In n -GaAs near the $E_0+\Delta_0$ gap it was found that the LOPCM peaks occurred at lower frequencies in polarization configurations where the interference between scattering mechanisms is allowed.²³ This effect could account for the additional downward shift observed in the NIR spectra of the L^- modes.

C. Raman signal from LO modes

The origin of the feature that is observed in the LO mode spectral region in all Raman spectra of high-quality n -InN is not clear. In previous works this Raman peak was assigned to the unscreened $A_1(\text{LO})$ mode.^{9,33} Other authors have recently attributed this feature to large wave-vector L^- coupled-mode scattering where the wave-vector nonconservation is induced by elastic scattering by impurities.^{13,14,16,17} It should be noted that the prevalence of these processes requires very high impurity concentrations.³⁴ In view of the L^- mode behavior observed in our samples, which displays both the usual free-charge and wave-vector dependence for a long-wavelength LOPCM, we believe that wave-vector nonconserving scattering by LOPCMs is unlikely to play a predominant role in the high-quality samples used in this study.

It has been recently established that, unlike most III-V semiconductors, wurtzite InN exhibits electron accumulation at the surface.¹⁻³ The only other case of III-V material reported to display an accumulation layer is InAs.³⁵ The surface electron density is however much higher in the case of InN.^{2,4} Interestingly, the Raman spectrum of n -type InAs also exhibits a sharp peak at the frequency of the LO mode, which was attributed to unscreened LO scattering at large wave vectors within the accumulation layer.³⁶ In the case of InN, it has been estimated that the electron-density peaks at a depth of ≈ 4 Å and then falls to the bulk density over 80 Å.^{2,4} This leads to confining electric fields in excess of 10^6 V cm⁻¹ for depths down to ~ 20 Å. Considering an effective depth of the accumulation layer of $d_s \sim 20$ Å, we estimate a scattering wave-vector uncertainty $\Delta q \sim 2/d_s \sim 10^7$ cm⁻¹. For wave vectors larger than the Thomas-Fermi wave vector the free carriers cannot screen the electric field of the LO phonons and these large- q modes are effectively decoupled from the electron plasma. Then, scattering by LO phonons at large wave vectors which are unscreened may explain the relatively intense LO signal usually observed in Raman scattering studies of n -InN layers.^{9,10,14,16-18}

To investigate in more detail the LO spectral region we have carried out Raman spectra using visible and NIR excitation light. Figure 6 shows the Raman spectra in the LO region for sample A4 taken under 514.5- and 780-nm-wavelength excitations. Similar spectra are obtained for all the InN layers. For comparison purposes, the overall intensity of the respective spectra was normalized to the E_2^{high} intensity. The spectrum taken under 514.5 nm excitation shows a peak at 592 cm⁻¹ with a shoulder on its high-frequency side. In earlier studies a hypothetical surface depletion layer was assumed,¹⁷ and it was concluded that the presence of a surface depletion layer that could explain the observation of the unscreened $A_1(\text{LO})$ mode could be ruled out. In view of more recent data which have established the unique properties of the InN surface such as an extreme electron accumulation, we attribute the peak at 592 cm⁻¹ to unscreened $A_1(\text{LO})$ scattering at large wave vectors in the surface accumulation layer, which, as discussed above, is decoupled from the electron plasma. Furthermore, the extremely high electric fields associated with the confining potential in the accumulation layer favor the field-induced scattering mechanisms, which results in a strong enhancement of

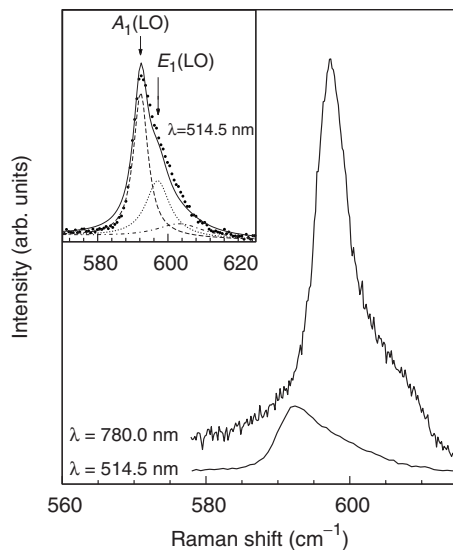


FIG. 6. Raman spectra of sample A2 obtained at 80 K under 514.5- and 780.0-nm-wavelength excitations in the spectral region of the LO modes. Inset: decomposition of the LO signal into $A_1(\text{LO})$ and $E_1(\text{TO})$ components for the 514.5 nm excitation spectrum.

the $A_1(\text{LO})$ peak from the accumulation layer.

In the inset of Fig. 6 we show the decomposition of the LO Raman peak into three Lorentzian line-shape components. In addition to a very weak, broad peak located at 603 cm^{-1} which is probably related to defects, the line-shape fit yields two main peaks: a dominant peak at 592 cm^{-1} corresponding to the $A_1(\text{LO})$ mode and a weaker peak at 597 cm^{-1} . An estimation for the $A_1(\text{LO})$ mode full width at half maximum of $\approx 5 \text{ cm}^{-1}$ was obtained from this fit. We tentatively assign the peak at 597 cm^{-1} to the $E_1(\text{LO})$ mode, which may appear in the spectrum because of the relaxation of selection rules induced by defects. An analogous situation occurs in other III-V doped semiconductors such as GaAs, where the observation of forbidden TO modes was ascribed to impurity scattering.²³ In wurtzite structure this effect can excite $E_1(\text{LO})$ modes, which display a strong intraband Fröhlich interaction and may become visible in the Raman spectra. In fact, as can be seen in Fig. 6, a strong enhancement of the LO signal is obtained by using the 780 nm excitation. Remarkably, the LO Raman peak in the NIR spectrum is observed at 597 cm^{-1} , that is, at the $E_1(\text{LO})$ frequency. We speculate that this observation might be accounted for by considering two aspects of the NIR Raman measurements. First, the probing depth of the 780 nm excitation is about two times that of the 514.5 nm excitation. As a consequence, the NIR spectra contain a significantly larger contribution from the “bulk” InN film where the $A_1(\text{LO})$ mode is coupled with the longitudinal plasma oscillations and therefore does not yield unscreened $A_1(\text{LO})$ scattering. Second, the 780 nm excitation is closer to an electronic criti-

cal point and this gives rise to a strong enhancement of the $E_1(\text{LO})$ mode which, being transverse to the plasma oscillations, remains uncoupled also in the bulk region of the InN film and dominates the spectrum. Owing to the increased probing depth, the defect-related feature is clearly visible on the high-frequency side, and its intensity is higher in samples with higher free-electron density, reflecting the increased density of defects in those samples.

V. CONCLUSION

The L^- LOPCM Raman peak was observed in Raman scattering measurements performed on a series of intentionally undoped n -type InN layers with free-electron densities spanning a 1 order of magnitude range and displaying high mobility and good crystalline quality. By studying the free-electron-density dependence as well as the wave-vector dependence of this peak, we show that it arises from wave-vector conserving scattering by long-wavelength L^- coupled modes. The corresponding L^+ mode is not detected, probably due to inhomogeneous broadening and low signal levels. The dependence of the L^- Raman peak on free-electron density has been successfully modeled using the standard dielectric theory in the Hon-Faust formalism and the Lindhard-Mermin model for the electronic susceptibility. The electron densities derived from line-shape fits to the Raman spectra agree well with the Hall-effect determinations.

These results show that Raman scattering by long-wavelength LOPCMs takes place in InN layers with good crystallinity. This is in contrast with previous studies of LO-phonon-plasmon coupling in InN that invoked the dominance of large wave-vector scattering processes to explain the Raman spectra of n -InN layers. The wave-vector conserving character of the Raman scattering by LOPCMs observed in our samples is corroborated by Raman scattering measurements performed under 780 nm excitation. In these experiments, a resonant enhancement of the polar modes is observed. The reduction in excitation wave vector causes the L^- modes to shift to lower frequencies in NIR spectra as compared to the visible spectra. The observed frequency shifts are in reasonable agreement with those expected from the well-known wave-vector dispersion of the LOPCMs, which provides a further indication that wave-vector conserving scattering by LOPCMs takes place. The presence of a relatively strong unscreened LO Raman signal in the spectra is attributed to surface-field-induced Raman scattering in the accumulation layer, where the wave-vector uncertainty favors scattering by unscreened large wave-vector LO modes.

ACKNOWLEDGMENTS

This work has been supported by the Spanish Ministry of Science and Innovation under contract MAT2007-63617 and by FPI and Ramón y Cajal Programs.

- ¹H. Lu, W. J. Schaff, L. F. Eastman, and C. E. Stutz, *Appl. Phys. Lett.* **82**, 1736 (2003).
- ²I. Mahboob, T. D. Veal, C. F. McConville, H. Lu, and W. J. Schaff, *Phys. Rev. Lett.* **92**, 036804 (2004).
- ³I. Mahboob, T. D. Veal, L. F. J. Piper, C. F. McConville, H. Lu, W. J. Schaff, J. Furthmüller, and F. Bechstedt, *Phys. Rev. B* **69**, 201307(R) (2004).
- ⁴T. D. Veal, L. F. J. Piper, W. J. Schaff, and C. F. McConville, *J. Cryst. Growth* **288**, 268 (2006).
- ⁵*Light Scattering in Solids IV*, Topics in Applied Physics, edited by M. Cardona and G. Güntherodt (Springer-Verlag, Berlin, 1984), Vol. 54.
- ⁶L. Artús, R. Cuscó, J. Ibáñez, N. Blanco, and G. González-Díaz, *Phys. Rev. B* **60**, 5456 (1999).
- ⁷R. Cuscó, J. Ibáñez, and L. Artús, *Phys. Rev. B* **57**, 12197 (1998).
- ⁸R. Cuscó, L. Artús, J. Ibáñez, N. Blanco, G. González-Díaz, M. Rahman, and A. R. Long, *J. Appl. Phys.* **88**, 6567 (2000).
- ⁹V. Y. Davydov, V. V. Emtsev, I. N. Goncharuk, A. N. Smirnov, V. D. Petrikov, V. V. Mamutin, V. A. Vekshin, S. V. Ivanov, M. B. Smirnov, and T. Inushima, *Appl. Phys. Lett.* **75**, 3297 (1999).
- ¹⁰T. Inushima, M. Higashiwaki, and T. Matsui, *Phys. Rev. B* **68**, 235204 (2003).
- ¹¹E. Kurimoto, M. Hangyo, H. Harima, M. Yoshimoto, T. Yamaguchi, T. Araki, and a. K. K. Y. Nanishi, *Appl. Phys. Lett.* **84**, 212 (2004).
- ¹²Y. M. Chang, C. T. Chuang, C. T. Chia, K. T. Tsen, H. Lu, and W. J. Schaff, *Appl. Phys. Lett.* **85**, 5224 (2004).
- ¹³J. S. Thakur, D. Haddad, V. M. Naik, R. Naik, G. W. Auner, H. Lu, and W. J. Schaff, *Phys. Rev. B* **71**, 115203 (2005).
- ¹⁴F. Demangeot, C. Piquier, J. Frandon, M. Gaio, O. Briot, B. Maleyre, S. Ruffenach, and B. Gil, *Phys. Rev. B* **71**, 104305 (2005).
- ¹⁵Y. M. Chang, H. W. Chu, C. H. Shen, H. Y. Chen, and S. Gwo, *Appl. Phys. Lett.* **90**, 072111 (2007).
- ¹⁶J. W. Pomeroy, M. Kuball, C. H. Swartz, T. H. Myers, H. Lu, and W. J. Schaff, *Phys. Rev. B* **75**, 035205 (2007).
- ¹⁷A. Kasic, M. Schubert, Y. Saito, Y. Nanishi, and G. Wagner, *Phys. Rev. B* **65**, 115206 (2002).
- ¹⁸S. Lazić, E. Gallardo, J. M. Calleja, F. Agulló-Rueda, J. Grandal, M. A. Sánchez-García, E. Calleja, E. Luna, and A. Trampert, *Phys. Rev. B* **76**, 205319 (2007).
- ¹⁹A. Kasic, E. Valcheva, B. Monemar, H. Lu, and W. J. Schaff, *Phys. Rev. B* **70**, 115217 (2004).
- ²⁰M. Kuball, N. Esser, T. Ruf, C. Ulrich, M. Cardona, K. Eberl, A. Garcia-Cristobal, and A. Cantarero, *Phys. Rev. B* **51**, 7353 (1995).
- ²¹M. Kuball, J. W. Pomeroy, M. Wintrebert-Fouquet, K. S. A. Butcher, H. Lu, W. J. Schaff, T. V. Shubina, S. V. Ivanov, A. Vasson, and J. Leymarie, *Phys. Status Solidi A* **202**, 763 (2005).
- ²²G. Irmer, V. V. Toporov, B. H. Bairamov, and J. Monecke, *Phys. Status Solidi B* **119**, 595 (1983).
- ²³V. Vorlíček, I. Gregora, W. Kauschke, J. Menéndez, and M. Cardona, *Phys. Rev. B* **42**, 5802 (1990).
- ²⁴M. V. Klein, B. N. Ganguly, and P. J. Colwell, *Phys. Rev. B* **6**, 2380 (1972).
- ²⁵D. T. Hon and W. L. Faust, *Appl. Phys. (Berlin)* **1**, 241 (1973).
- ²⁶R. Cuscó, L. Artús, S. Hernández, J. Ibáñez, and M. Hopkinson, *Phys. Rev. B* **65**, 035210 (2001).
- ²⁷X. Wang, S. B. Che, Y. Ishitani, and A. Yoshikawa, *Appl. Phys. Lett.* **89**, 171907 (2006).
- ²⁸J. Wu, W. Walukiewicz, W. Shan, K. M. Yu, J. W. Ager III, E. E. Haller, H. Lu, and W. J. Schaff, *Phys. Rev. B* **66**, 201403(R) (2002).
- ²⁹Q. Guo, O. Kato, M. Fujisawa, and A. Yoshida, *Solid State Commun.* **83**, 721 (1992).
- ³⁰E. O. Kane, *J. Phys. Chem. Solids* **1**, 249 (1957).
- ³¹J. Ibáñez, R. Cuscó, L. Artús, G. González-Díaz, and J. Jiménez, *Solid State Commun.* **121**, 609 (2002).
- ³²L. F. J. Piper, T. D. Veal, C. F. McConville, H. Lu, and W. J. Schaff, *Appl. Phys. Lett.* **88**, 252109 (2006).
- ³³M. C. Lee, H. C. Lin, Y. C. Pan, C. K. Shu, J. Ou, W. H. Chen, and W. K. Chen, *Appl. Phys. Lett.* **73**, 2606 (1998).
- ³⁴D. Olego and M. Cardona, *Phys. Rev. B* **24**, 7217 (1981).
- ³⁵D. C. Tsui, *Phys. Rev. Lett.* **24**, 303 (1970).
- ³⁶S. Buchner and E. Burnstein, *Phys. Rev. Lett.* **33**, 908 (1974).